Progress In Electromagnetics Research, PIER 88, 105–120, 2008

CURRENT DISTRIBUTIONS ALONG A RECEIVING THIN DIPOLE INSIDE IDEAL ANECHOIC AND REVERBERATION CHAMBERS

W. Y. Zhong and Z. X. Shen

School of Electrical and Electronic Engineering
Nanyang Technological University
50 Nanyang Avenue, Singapore 639798, Singapore

Y. K. R. Tai and W. J. Koh

DSO National Laboratories
20 Science Park Drive, Singapore 118230, Singapore

Abstract—This paper studies the correlation of a receiving thin dipole with an arbitrary load in both anechoic chamber (AC) and reverberation chamber (RC). In both cases, the method of moments is employed to calculate the current distributions along a thin dipole induced by external fields. In AC, a plane wave with a fixed incident angle and polarization is illuminated on the dipole; whereas in RC, the field is represented by an appropriate superposition of many incident plane waves with stochastic incident angles, polarizations and phases. Numerical results for the current distributions of a thin dipole with different loads and electrical lengths are presented and discussed in both chambers. It is demonstrated that the ratios with respect to current magnitudes at the arbitrary load of the thin dipole between AC and RC are determined by its directivity. In particular, the ratios with respect to current magnitudes along the entire dipole whose electrical length is less than half a wavelength are nearly constants regardless of the terminating load, which indicates that results obtained in both chambers are well correlated.

1. INTRODUCTION

Reverberation chamber (RC) is nowadays widely employed in many applications including aircraft, automotive, and wireless communication systems due to the availability of several military

and commercial standards, which provide measurement procedures for electromagnetic susceptibility and emission tests [1–8]. Basically, the RC is a three-dimensional metallic cavity containing rotation tuners, which are well-stirred to create a statistically uniform electromagnetic field environment. The total field in the chamber can be represented as many plane waves stochastically excited and superimposed whose distributions over incident angle, polarization, and phase are uniform.

Recently, specific effort has been made on the issue with respect to the correlation between an RC and conventional anechoic chamber (AC). This research topic has significantly constructive and standardized values, i.e., the experimental methods could be interchanged and selected where appropriate in terms of the different category of equipment under test (EUT) and its specific working electromagnetic environment applying the existing correlation coefficients between AC and RC. A statistical correlation [9] between AC and RC was demonstrated to be possible in automotive applications. A statistical theory [10] for assessing the directivity of emitters based on the electrical size of the device was reported. Test article response and its uncertainty [11] were compared in anechoic and reverberation chambers. A better correlation [12] based on a statistical approach could be obtained by applying the transfer function of electronic devices.

From published papers, it is seen that no general conclusion has been drawn with respect to the correlation of test results in both AC and RC. It appears apparent that some theoretical analysis is required to characterize this correlation more accurately and to provide basic insight into this correlation. In this paper, a receiving straight thin dipole with an arbitrary load is selected to study its current distributions both in AC and RC. Our objective is not only to model the current distributions along a thin dipole in both chambers, but also to find the possible correlation between AC and RC from the theoretical point of view.

The organization of the present paper is as follows. In Section 2, the theoretical formulation is briefly described. In Section 3, numerical results are presented and discussed. Conclusions about the correlation of AC and RC are drawn in Section 4.

2. FORMULATION

In this section, we consider a receiving antenna placed in anechoic and reverberation chambers. The simple case of a perfectly conducting thin dipole with an arbitrary load will be considered here though it may be easily extended to other situations. We will employ the

dependently extracted method [13] to create a set of plane waves with an uniformly distributed random incidence to simulate the statistically uniform electromagnetic environment in an RC.

Figure 1 shows a straight thin dipole with length l and radius a center-loaded by an arbitrary impedance Z_L. Here we are interested in finding the correlation coefficient between current magnitudes along the dipole induced by external fields in anechoic and reverberation chambers.

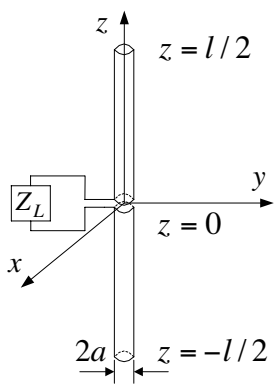

Figure 1. Geometry of a thin dipole with an arbitrary load.

2.1. Dipole in Anechoic Chamber

Figure 2 shows the thin dipole placed in an anechoic chamber and illuminated by a plane wave of certain incident angle and polarization. Following Eq. (14) in [14], it is known that the total receiving current $I^r(z)$ along the thin dipole with an arbitrary load is represented by

$$I^r(z) = I_0^r(z) - \frac{Z_0 \cdot Z_L}{Z_0 + Z_L} I_0^r(0) \cdot I_t(z) \tag{1}$$

where $I_0^r(z)$ refers to the receiving current distribution in the absence of the load ($Z_L = 0$), $I_t(z)$ denotes the transmitting current distribution excited by voltage generator of unit strength (1 V/m) and Z_0 is the feed-point impedance of the thin dipole.

Using the method of moments [15–19], one can solve the current distributions $I_0^r(z)$ and $I_t(z)$ along the thin dipole, respectively. Following the procedures used in [20], one can easily obtain the following

$$[I] = [Z]^{-1} [V] \tag{2}$$

where

$$Z_{mn} = j\omega\mu\Delta l_n \cdot \Delta l_m \psi(n,m) + \frac{1}{j\omega\varepsilon}\left[\psi(n^+,m^+) - \psi(n^-,m^+) - \psi(n^+,m^-) + \psi(n^-,m^-)\right] \tag{3}$$

$$\psi(n,m) = \begin{cases} \dfrac{1}{2\pi\Delta l_n}\log\left(\dfrac{\Delta l_n}{a}\right) - \dfrac{jk}{4\pi} & n = m \\ \dfrac{e^{-jkR_{mn}}}{4\pi R_{mn}} & n \neq m \end{cases} \tag{4}$$

$$[V_0] = \begin{pmatrix} \bar{E}^i(1)\cdot\Delta\bar{l}_1 \\ \bar{E}^i(2)\cdot\Delta\bar{l}_2 \\ \bar{E}^i(3)\cdot\Delta\bar{l}_3 \\ \vdots \\ \bar{E}^i(N)\cdot\Delta\bar{l}_N \end{pmatrix} [V_t] = \begin{pmatrix} 0 \\ \vdots \\ 1 \\ \vdots \\ 0 \end{pmatrix} \tag{5}$$

V_0 and V_t are the voltage excitations of the receiving dipole with no load and the transmitting dipole, respectively.

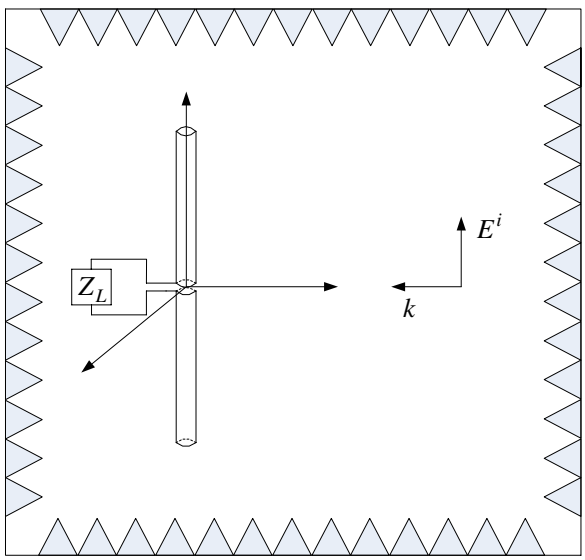

Figure 2. A thin dipole illuminated by a plane wave with a fixed incident angle and polarization in AC.

For a plane wave incidence in AC shown in Fig. 2, we set

$$\bar{E}^i(n) = \bar{E}_0 e^{-j\bar{k}\cdot\bar{r}} \tag{6}$$

where the propagation constant $\bar{k}$ is

$$\bar{k} = -k(\sin\theta\cos\phi\hat{a}_x + \sin\theta\sin\phi\hat{a}_y + \cos\theta\hat{a}_z) \tag{7}$$

and $\bar{E}_0$ is the electric field intensity of the incident plane wave. In AC, the obtained current magnitude should be normalized by the electric field intensity around the dipole. In this paper, we set $E_0 = 1\,\mathrm{V/m}$.

It is well known that the effective area A_e of an antenna can be expressed as [21]

$$A_e(\Omega) = \frac{\lambda^2}{4\pi} D(\theta,\phi) p m \eta_a \tag{8}$$

where p is the polarization mismatch, m the impedance mismatch, η_a the antenna efficiency, and $D(\theta,\phi)$ the antenna directivity. The received power at the load Z_L of the thin dipole shown in Fig. 2 is then

$$(P_L)_{AC} = \frac{E_{AC}^2}{\eta} A_e = \frac{E_{AC}^2}{\eta}\frac{\lambda^2}{4\pi} D(\theta,\phi) m \eta_a \tag{9}$$

where E_{AC}^2/η can be interpreted as the scalar power density, $p = 1$ is assumed here because only the polarization of the incident wave in the plane containing its propagation direction and dipole is considered. Thus, the normalized received power of the thin dipole with respect to the term of E_{AC}^2 in AC is as follows

$$((P_L)_{AC})_{norm} = \frac{(P_r)_{AC}}{E_{AC}^2} = \frac{1}{\eta}\frac{\lambda^2}{4\pi} D(\theta,\phi) m \eta_a \tag{10}$$

2.2. Dipole in Reverberation Chamber

The electric field $\bar{E}$ in a source-free working volume of an RC can be represented as an integral of plane waves over all real solid angles [22, 23]

$$\bar{E}^i(\bar{r}) = \int_{4\pi} \bar{E}_0(\Omega) e^{-j\bar{k}\cdot\bar{r}} d\Omega \tag{11}$$

where the solid angle is shorthand for the elevation angle θ and azimuth angle ϕ, and $d\Omega = \sin\theta d\theta d\phi$. Vector $\bar{k}$ is the propagation vector of the same expression as (7).

Define a new Cartesian coordinate system $(\hat{a}_{x'}, \hat{a}_{y'}, \hat{a}_{z'})$ with the z' axis in accordance with the propagation vector $\bar{k}$. The new and original coordinate systems are related to each other through a rotation matrix $[T]$ in the following form

$$\begin{bmatrix} \hat{a}_{x'} \\ \hat{a}_{y'} \\ \hat{a}_{z'} \end{bmatrix} = [T] \begin{bmatrix} \hat{a}_x \\ \hat{a}_y \\ \hat{a}_z \end{bmatrix} \tag{12}$$

where

$$[T] = \begin{bmatrix} \cos\theta\cos\phi & \cos\theta\sin\phi & -\sin\theta \\ -\sin\phi & \cos\phi & 0 \\ \sin\theta\cos\phi & \sin\theta\sin\phi & \cos\theta \end{bmatrix} \tag{13}$$

Due to the fact that the plane wave spectrum $\bar{E}_0(\Omega)$ is a random variable, it can be written in the new coordinate system as defined above

$$\bar{E}_0(\Omega) = \left|\bar{E}_0\right| \left(\hat{a}_{x'} \cos\alpha + \hat{a}_{y'} \sin\alpha\right) \tag{14}$$

where α is the polarization angle of the electric field in the plane that is perpendicular to $\bar{k}$. Utilizing the rotation matrix (13), (14) can be easily expressed in the original coordinate system as follows

$$\begin{aligned} \bar{E}_0(\Omega) \;=\; & \left|\bar{E}_0\right| [(\cos\theta\cos\phi\cos\alpha - \sin\phi\sin\alpha)\hat{a}_x \\ & +(\cos\theta\sin\phi\cos\alpha + \cos\phi\sin\alpha)\hat{a}_y - (\sin\theta\cos\alpha)\hat{a}_z] \end{aligned} \tag{15}$$

For a statistically uniform field as created in an RC, the angular spectrum is considered to be a random variable due to the different boundary conditions, which depend on different stirrer positions. For calculating the current distribution along a receiving thin dipole, the theory of probability is employed. That is to say, a certain number of random plane waves with stochastic phases are assumed to impinge upon the dipole antenna simultaneously, for which the vector propagation direction and the angular spectrum are random but orthogonal.

Referring to Fig. 3, the random parameters are angles ϕ and θ defining the propagation direction of the incident plane wave, polarization angle α and the phase of the incident wave ξ. Following the procedure in [13], an uniform distribution of the extracted points can be acquired on the spherical surface. The average total field within the working volume of an RC [24] can be calculated in terms of the superposition of N random plane waves with equal magnitude E_0 in the following

$$\langle |E_{RC}| \rangle = \frac{15}{16}\sqrt{\frac{\pi}{3}}\sqrt{N}\,|E_0| \tag{16}$$

Herein, M simulations are conducted in order to simulate M different stirrer positions in a real RC. Each simulation consists of the superposition of N random plane waves whose incidences, polarizations and phases are all stochastic. Following various validations [13] and applying the law of large numbers, a compromise is made between accuracy and computation time with respect to the choices of N and M over the whole frequency band of interest including the lowest usable frequency (LUF). Here, we choose $N = 200$ and $M = 500$,

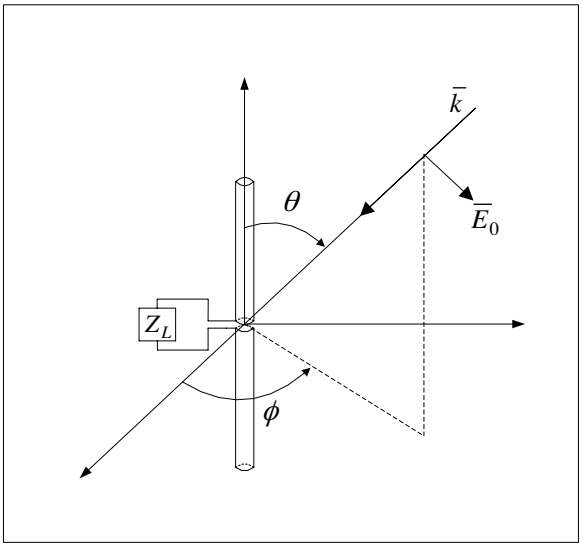

Figure 3. One random plane wave in RC. The vector propagation constant and the electric field polarization are orthogonal.

which can sufficiently ensure convergent results within the acceptable computation time. In RC, numerical normalizations are made by taking the ratio between the current magnitudes and the average total field around the dipole. For computational convenience, the total field is obtained applying (16) with $E_0 = 1\,\mathrm{V/m}$.

Through the analysis and superposition assumptions above, the induced current along the thin dipole with an arbitrary load employing the numerical method can be expressed as follows

$$|I_{RC}| = \frac{1}{M}\sum_{1}^{M}\left|\sum_{1}^{N}\bar{I}_e\right| \tag{17}$$

where $\bar{I}_e$ is the vector current along the thin dipole illuminated by each random incident plane wave.

In this paper, $\langle\rangle$ represents an ensemble average over stirrer positions. Referring to [22], the average received power at the terminating load of the thin dipole in RC is in the following

$$\langle P_L\rangle_{RC} = \frac{\left\langle |E_{RC}|^2\right\rangle}{\eta}\langle A_e\rangle = \frac{|E_{RC}|^2}{\eta}\frac{\lambda^2}{8\pi}m\eta_a \tag{18}$$

where $\left\langle |E_{RC}|^2\right\rangle\Big/\eta$ can be interpreted as the average scalar power

density. Thus, the normalized average received power of the thin dipole with respect to the term of $\left\langle |E_{RC}|^2 \right\rangle$ in RC is as follows

$$(\langle P_L \rangle_{RC})_{norm} = \frac{\langle P_r \rangle_{RC}}{\left\langle |E_{RC}|^2 \right\rangle} = \frac{1}{\eta} \frac{\lambda^2}{8\pi} m \eta_a \tag{19}$$

2.3. Current Ratio

Combining (10) and (19) yields the normalized received power ratio at the load of the thin dipole between AC and RC.

$$\frac{((P_L)_{AC})_{norm}}{(\langle P_L \rangle_{RC})_{norm}} = 2D(\theta, \phi) \tag{20}$$

Therefore, using the expression of $P_L = I_L^2 \cdot Z_L$, it is apparent that

$$\frac{((I_L)_{AC})_{norm}}{(\langle I_L \rangle_{RC})_{norm}} = \sqrt{2D(\theta, \phi)} \tag{21}$$

Herein, $(I_L)_{norm}$ refers to the normalized current magnitude at the load of the thin dipole and their ratio is independent of the terminating load impedance Z_L.

3. NUMERICAL RESULTS

Figures 4, 5, and 6 present the normalized current distributions along a thin dipole of different electrical lengths with different loads (conjugate-matched, open-circuited and short-circuited ones) in AC and RC, respectively. By default, the current magnitudes in this paper refer to the normalized values and the direction of the incident wave in AC is chosen to be perpendicular to the thin dipole unless otherwise stated. In Figs. 5(b)–(c), we compare our numerical results with those obtained by IE3D and the agreement between them is very good. From Figs. 4 and 5, it is found that the current magnitude values along the length of dipole in AC are always larger than the ones in RC when the electrical length of the dipole is less than half a wavelength.

Table 1 presents the current magnitude ratio at the load of a thin dipole illuminated by signals with different frequencies (i.e., different electrical lengths) between anechoic and reverberation chambers. From the table, it is evidently shown that our numerical results are in excellent agreement with theoretical results obtained in [22]. It should be mentioned that the current ratio at the load is independent upon the dipole load and determined by the directivity of the dipole.

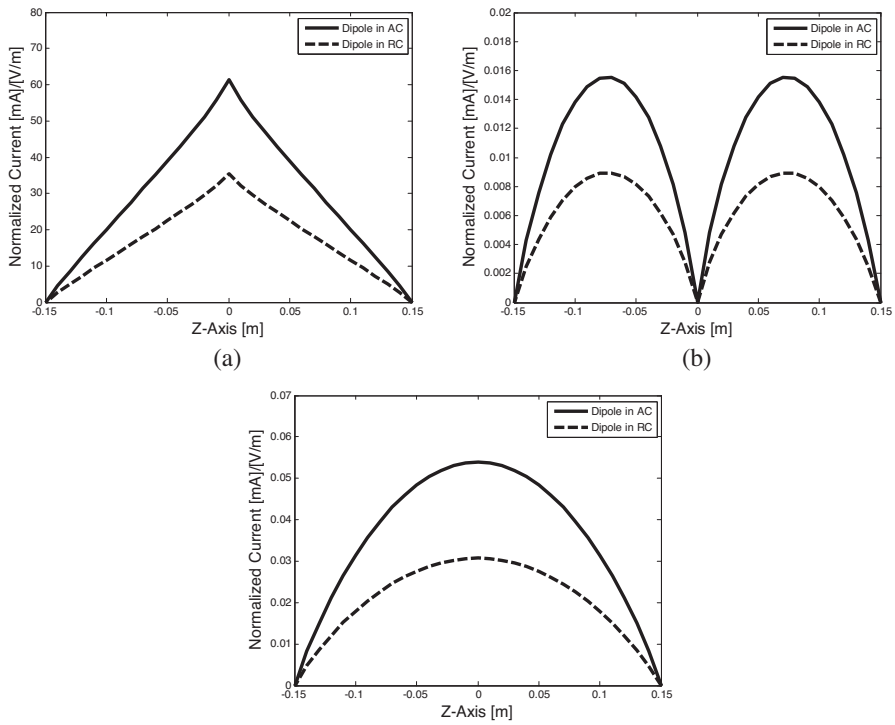

Figure 4. Normalized current distributions along a thin dipole in AC and RC ($l/2a = 1e3$, $l = 0.08\lambda$, $Z_0 = R - jX$, $R = 1.181\,\Omega$, $X = 2691\,\Omega$). (a) $Z_L = Z_0^*$. (b) $Z_L = 1e10\,\Omega$. (c) $Z_L = 0\,\Omega$.

Table 1. Normalized current magnitude ratios at the load of a thin dipole between AC and RC.

Frequency (MHz)	80	250	500	750	1000	1250
Electrical Length	0.08λ	0.25λ	0.50λ	0.75λ	λ	1.25λ
Directivity (D)	1.50	1.55	1.67	1.90	2.41	3.28
$\sqrt{2D}$(Theoretical Result)	1.73	1.76	1.83	1.95	2.20	2.56
Our Numerical Result	1.74	1.79	1.87	1.98	2.30	2.75

Figure 7 depicts their normalized current magnitude ratios between AC and RC along the dipole terminated by different loads with respect to different electrical lengths of the dipole. It is easily

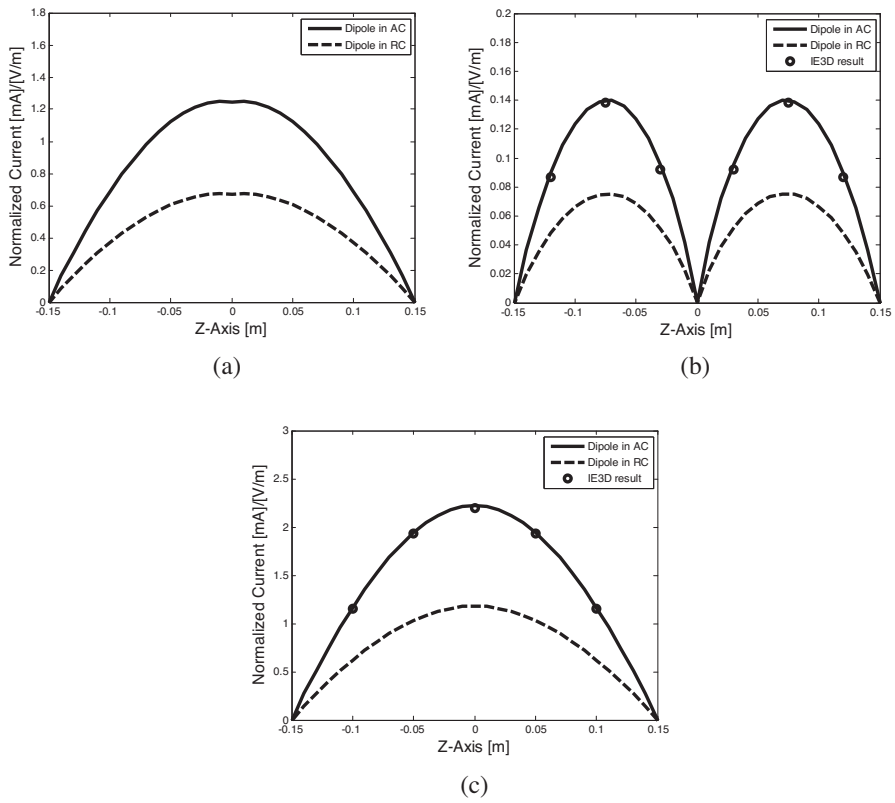

Figure 5. Normalized current distributions along a thin dipole in AC and RC ($l/2a = 1e3$, $l = 0.5\lambda$, $Z_0 = R + jX$, $R = 80.52\,\Omega$, $X = 40.77\,\Omega$). (a) $Z_L = Z_0^*$. (b) $Z_L = 1e10\,\Omega$. (c) $Z_L = 0\,\Omega$.

seen that the ratios are constants, approximately 1.74 for $l = 0.08\lambda$ and 1.87 for $l = 0.5\lambda$, along the entire length of the dipole when the electrical length of a dipole is less than half a wavelength. It is easy to understand that the ratio is a constant for a particular short dipole because of the nearly sinusoidal variation of the current distribution along a short dipole. Furthermore, this constant is determined by the directivity of the thin dipole at the elevation angle of the incident plane wave in AC.

From Fig. 7(c), it is apparently seen that current magnitude ratios along the length of a full-wavelength dipole are no longer constant, which mainly depends upon the different terminating loads. Similarly to the results given in [14], the current distribution along a full-

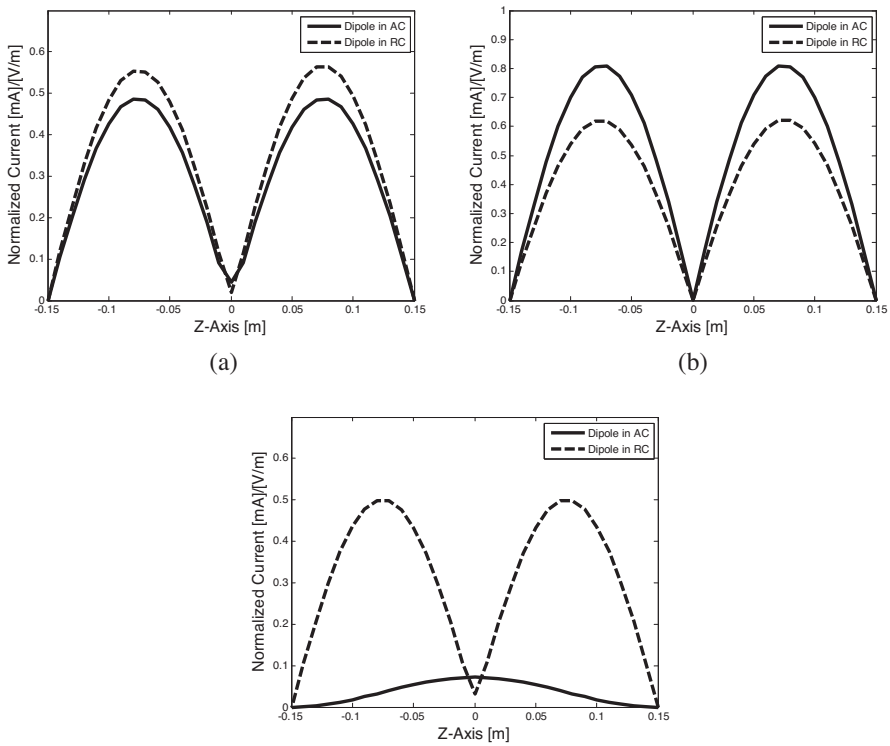

Figure 6. Normalized current distributions along a thin dipole in AC and RC ($l/2a = 1e10$, $l = \lambda$, $Z_0 = R - jX$, $R = 22896\,\Omega$, $X = 16801\,\Omega$). (a) $Z_L = Z_0^*$. (b) $Z_L = 1e10\,\Omega$. (c) $Z_L = 0\,\Omega$.

wavelength dipole with a short-circuited load is shown in Fig. 8 in the case of different incident angles. For normal incidence, the peak current magnitude exists at the center of the dipole. From Fig. 8, it is easily found that the current distribution along the full-wavelength dipole will change when the incident angle varies and this is mainly due to the reversed phases along the dipole. As we know, the electromagnetic environment in RC consists of many random incident waves, which lead to a current dip at the center of the thin full-wavelength dipole with a short-circuited load, unlike that under the normal incidence in AC, as shown Fig. 6(c). Therefore, the ratio of the current magnitudes along a thin full-wavelength dipole is no longer a constant. However, the current magnitude ratios at the load of a full-wavelength dipole are still constant of 2.3, as shown in Table 1, which is determined by

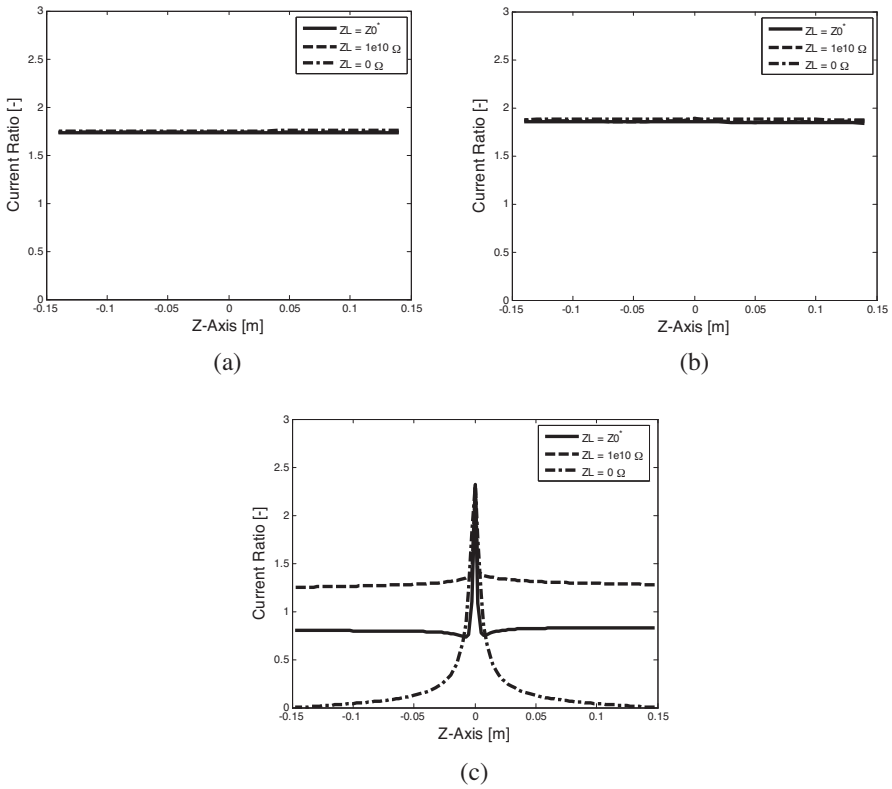

Figure 7. Normalized current magnitude ratios along a thin dipole in AC and RC. (a) $l = 0.08\lambda$. (b) $l = 0.5\lambda$. (c) $l = \lambda$.

the directivity. Actually, it is easy to find that the current magnitude ratio along the length of a thin dipole between AC and RC began to be not a constant as the electrical length of dipole is more than half a wavelength.

Finally, the current distributions along a thin half-wavelength dipole with a conjugate-matched load illuminated by different incidences in AC and compared with that in RC are provided in Fig. 9. For incidences not perpendicular to the thin dipole, the induced current distributions along the thin dipole are shown to be asymmetric as expected, which leads to the fact that the current magnitude ratios along the thin dipole between AC and RC are no longer constants, as shown in Fig. 10.

It is well known the directivity of a half-wavelength dipole can be

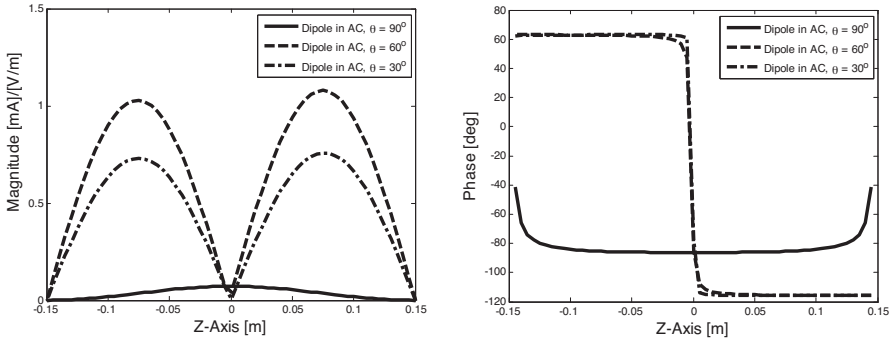

(a) (b)

Figure 8. Normalized current distributions along a thin dipole in AC in the case of different incident angles ($l/2a = 1e10$, $l = \lambda$, $Z_L = 0\,\Omega$). (a) Magnitudes. (b) Phases.

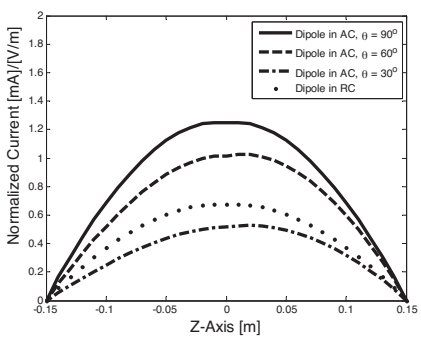

Figure 9. Normalized current distributions along a thin dipole in AC with different incidences and RC ($l/2a = 1e3$, $l = 0.5\lambda$, $Z_L = Z_0^*$).

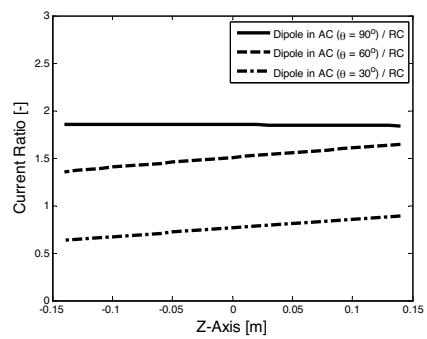

Figure 10. Normalized current magnitude ratios along a thin dipole in AC with different incidences and RC ($l/2a = 1e3$, $l = 0.5\lambda$, $Z_L = Z_0^*$).

approximated using Eq. (2.18) in [25]

$$D = D_0 \sin^3\theta = 1.67 \sin^3\theta \tag{22}$$

where θ is the elevation angle. Therefore, varying the direction of incident wave in AC, different current magnitude ratios at the load of the half-wavelength dipole between AC and RC will be obtained due to the different directivity at the specific elevation angle.

Table 2 presents the normalized current magnitude ratios at the terminating load of a thin half-wavelength dipole with a conjugate-matched load at different incident angles between AC and RC, which validates the conclusions drawn in this paper. It is clearly seen that the maximum current magnitude ratio will be obtained if the direction of the incident wave is perpendicular to the thin half-wavelength dipole in AC. In addition, there exists a relatively acceptable error between our numerical result and theoretical result when the incidence is near grazing, which might be due to the approximated directivity formula.

Table 2. The normalized current magnitude ratios at the load of a thin half-wavelength dipole with a conjugate-matched load in AC with different incidences and RC.

Incidence in AC	90°	60°	30°
Directivity (D)	1.67	1.08	0.21
$\sqrt{2D}$(Theoretical Result)	1.83	1.47	0.65
Our Numerical Result	1.87	1.51	0.77

4. CONCLUSIONS

In this paper, the current distributions along a receiving thin dipole inside AC and RC have been presented and discussed. It has been demonstrated that the ratios with respect to current magnitudes at the arbitrary load of the thin dipole between AC and RC have been determined by the directivity of the thin dipole. In particular, the current magnitude ratios along the entire dipole less than half a wavelength are nearly constants, which indicates that results obtained in AC and RC are well correlated.

REFERENCES

1. Corona, P., G. Latmiral, E. Paolini, and L. Piccioli, "Use of a reverberating enclosure for measurements of radiated power in the microwave range," *IEEE Trans. Electromagn. Compat.*, Vol. 18, No. 2, 54–59, 1976.
2. Corona, P., G. Latmiral, and E. Paolini, "Performance and analysis of a reverberating enclosure with variable geometry," *IEEE Trans. Electromagn. Compat.*, Vol. 22, No. 1, 2–5, 1980.

3. Ma, M., "Understanding reverberating chambers as an alternative facility for EMC testing," *Journal of Electromagnetic Waves and Applications*, Vol. 2, No. 3–4, 339–351, 1988.
4. Rahman, H., "Electromagnetic susceptibility of a folded cable of finite thickness in a shielded enclosure to external excitation," *Journal of Electromagnetic Waves and Applications*, Vol. 12, No. 10, 1349–1356, 1998.
5. Hatfield, M., "Status of reverberation chamber standards," *Proc. IEEE Int. Symp. EMC*, 279–281, 2003.
6. Kouveliotis, N., P. Trakadas, and C. Capsalis, "FDTD modeling of a vibrating intrinsic reverberation chamber," *Progress In Electromagnetics Research*, PIER 39, 47–59, 2003.
7. Wang, Y., W. Koh, and C. Lee, "Coupling cross section and shielding effectiveness measurements on a coaxial cable by both mode-tuned reverberation chamber and gtem cell methodologies," *Progress In Electromagnetics Research*, PIER 47, 61–73, 2004.
8. Zhao, H. and Z. Shen, "Modal-expansion analysis of a monopole in vibrating reverberation chamber," *Progress In Electromagnetics Research*, PIER 85, 303–322, 2008.
9. Musso, L., F. Canavero, B. Demoulin, and V. Berat, "Radiated immunity testing of a device with an external wire: Repeatability of reverberation chamber results and correlation with anechoic chamber results," *Proc. IEEE Int. Symp. EMC*, 828–833, 2003.
10. Koepke, G., D. Hill, and J. Ladbury, "Directivity of the test device in EMC measurement," *Proc. IEEE Int. Symp. EMC, Reverberation Chamber Workshop*, 535–539, 2000.
11. Freyer, G. and M. Backstrom, "Comparison of anechoic and reverberation chamber coupling data as a function of directivity pattern," *Proc. IEEE Int. Symp. EMC*, 615–620, 2000.
12. Freyer, G. and M. Backstrom, "Impact of equipment response characteristics on anechoic and reverberation chamber test results," *Proc. EMC Europe, Int. Symp. Electromagnetic Compatibility*, Vol. 1, 51–55, 2002.
13. Moglie, F. and A. Pastore, "FDTD analysis of plane waves superposition to simulate susceptibility tests in reverberation chambers," *IEEE Trans. Electromagn. Compat.*, Vol. 48, No. 1, 195–202, 2006.
14. Chang, D., S. Lee, and L. Rispin, "Simple formula for current on a cylindrical receiving antenna," *IEEE Trans. Antennas Propagat.*, Vol. 26, No. 5, 683–690, 1978.
15. Huang, E. and A. Fung, "An application of sampling theorem

to moment method simulation in surface scattering," *Journal of Electromagnetic Waves and Applications*, Vol. 20, No. 4, 531–546, 2006.

16. Selcuk, A. and B. Saka, "A general method for the analysis of curved wire antennas," *Journal of Electromagnetic Waves and Applications*, Vol. 21, No. 2, 175–188, 2007.
17. Su, C. and T. Sarkar, "A new formula for the evaluation of the impedance matrix in the method of moments," *Progress In Electromagnetics Research*, PIER 22, 85–105, 1999.
18. Lashab, M., F. Benabdelaziz, and C.-E. Zebiri, "Analysis of electromagnetics scattering from reflector and cylindrical antennas using wavelet-based moment method," *Progress In Electromagnetics Research*, PIER 76, 357–368, 2007.
19. Hatamzadeh-Varmazyar, S., M. Naser-Moghadasi, and Z. Masouri, "A moment method simulation of electromagnetic scattering from conducting bodies," *Progress In Electromagnetics Research*, PIER 81, 99–119, 2008.
20. Harrington, R., *Field Computation by Moment Methods*, Macmillan, New York, 1968.
21. Tai, C., "On the definition of effective aperture of antennas," *IEEE Trans. Antennas Propagat.*, Vol. 9, 224–225, 1961.
22. Hill, D., "Plane wave integral representation for fields in reverberation chambers," *IEEE Trans. Electromagn. Compat.*, Vol. 40, No. 3, 209–217, 1998.
23. Hill, D., "Spatial correlation function for fields in a reverberation chamber," *IEEE Trans. Electromagn. Compat.*, Vol. 37, No. 1, 138, 1995.
24. Musso, L., V. Berat, F. Canavero, and B. Demoulin, "A plane wave Monte Carlo simulation method for reverberation chambers," *Proc. EMC Europe, Int. Symp. Electromagnetic Compatibility*, Vol. 1, 45–50, 2002.
25. Balanis, C., *Antenna Theory: Analysis and Design*, 3rd edition, Wiley, New York, 2005.
26. Gronwald, F., "The influence of electromagnetic singularities on an active dipole antenna within a cavity," *Advances in Radio Science*, Vol. 1, 57–61, 2003.